Mechanochemical Coupling in Myosin: A Theoretical Analysis with Molecular Dynamics and Combined QM/MM Reaction Path Calculations

Guohui Li and Qiang Cui*

Department of Chemistry and Theoretical Chemistry Institute, University of Wisconsin, Madison, 1101 University Avenue, Madison, Wisconsin 53706

Received: October 20, 2003; In Final Form: January 6, 2004

To elucidate the detailed mechanism of ATP hydrolysis in myosin, molecular dynamics employing classical force field and reaction path analyses employing a combined quantum mechanical and molecular mechanical (QM/MM) potential were carried out. Although the QM/MM reaction path analyses have limited accuracy due to the lack of extensive conformational sampling, the present work showed that sensible energetics much closer to experimental measurements than previous computational studies can be obtained once the protein environment is included. In the two associative mechanisms studied here, the pathway that involves the conserved residue, Ser 236, as the proton relay group was found to have a lower rate-limiting barrier. However, it was also shown that if $O^{2\gamma}$ gets protonated, the mechanism without invoking any proton relay has only a slightly higher barrier and therefore may also contribute, especially in mutants such as Ser 236A. By performing calculations for two different motor domain conformations, it was shown that the mechanochemical coupling in myosin is mainly regulated by several residues in the switch I and switch II regions, such as Arg 238, Gly 457, and Glu 459. In particular, when the salt bridge between Arg 238 and Glu 459 is broken as in the prehydrolysis conformation of the motor domain, ATP hydrolysis is highly unfavorable energetically. In this conformation, Arg 238 is closer to ATP and therefore stabilizes the ATP state over the hydrolysis products. Moreover, without the salt bridge, the water structure in the active site is no longer stabilized to favor the in-line nucleophilic attack of the γ-phosphate. The results from the current work have general implications to other molecular motors that involve ATP hydrolysis, such as kinesin, F_1−ATPase and Ca^{2+}−ATPase, although more robust conclusions concerning the hydrolysis mechanism require more elaborate simulations that consider protein fluctuations and other possible protonation states of ATP and the hydrolysis products.

I. Introduction

Adenosine triphosphate (ATP) is commonly referred to as the fuel of life because its hydrolysis reaction is coupled to many processes in living systems that require energy input.[1] Important examples include the functional cycles of motor proteins, such as myosin,[2] kinesin,[3] and Ca^{2+}−ATPase,[4] which involve large scale conformational transitions upon ATP binding and/or hydrolysis. Therefore, it is of fundamental importance to reveal the mechanistic details of ATP hydrolysis in these systems and to understand how hydrolysis energetics are regulated by the conformation of the protein;[5,6] the coordination between ATP hydrolysis and conformational properties of the protein (i.e., mechanochemical coupling) is the key element for energy transductions in molecular motors.[7,8] Despite previous efforts, a mechanism with atomic details for such a fundamental reaction in the context of important biomolecular systems is still not available, and many proposals have been put forward (see below). In the current work, we employ both classical molecular dynamics[9] and combined quantum mechanical and molecular mechanical (QM/MM)[10−14] calculations to explore the mechanism of ATP hydrolysis in myosin-II. The results are expected to have important general implications to similar hydrolysis reactions in other proteins that involve ATP hydrolysis. These calculations are complemented with an analysis of the relative binding affinity of ATP and ADP + Pi to myosin using an alchemy free energy perturbation approach, which will be reported separately. These energetics-oriented studies explore different aspects of motor protein functions compared to previous work based on normal-mode analysis, which focused on the connection between conformational flexibilities of those systems (myosin-II,[15] Ca^{2+}−ATPase,[15,16] and F_1−ATPase[17]) and their functions.

Myosin-II (thereafter will be referred to as myosin) is one of the best-characterized molecular motors,[2,18−20] and has been the subject of diverse types of experimental studies for several decades. The functional cycle of the actin-myosin system has been established in an outline form, which is commonly known as the Lymn−Taylor model[21] or the Bagshaw−Trentham scheme.[22] As shown in Scheme 1, ATP binding induces the dissociation of myosin from the actin. Following a conformational change in the motor domain, ATP hydrolysis occurs with a nearly unity equilibrium constant ($K < 10$).[22] Subsequently, the motor domain reattaches the actin polymer at the next site, which induces the release of the hydrolysis products: inorganic phosphate and ADP. A conformational change ("power stroke") of myosin occurs during or after the release of ADP, which brings the myosin−actin system back to the rigor state. A large body of crystallographic,[23−29] electron microscopy,[30,31] mutagenesis,[32−35] and single molecule spectroscopy[36−39] studies have provided information with variable details into the structures of various intermediates and residues that make important contributions to the ATP hydrolysis. The remaining mysteries largely concern the binding interface between myosin

10.1021/jp0371783 CCC: $27.50 © 2004 American Chemical Society
Published on Web 02/17/2004

SCHEME 1. Functional Cycle of Myosin-II−Actin[a]

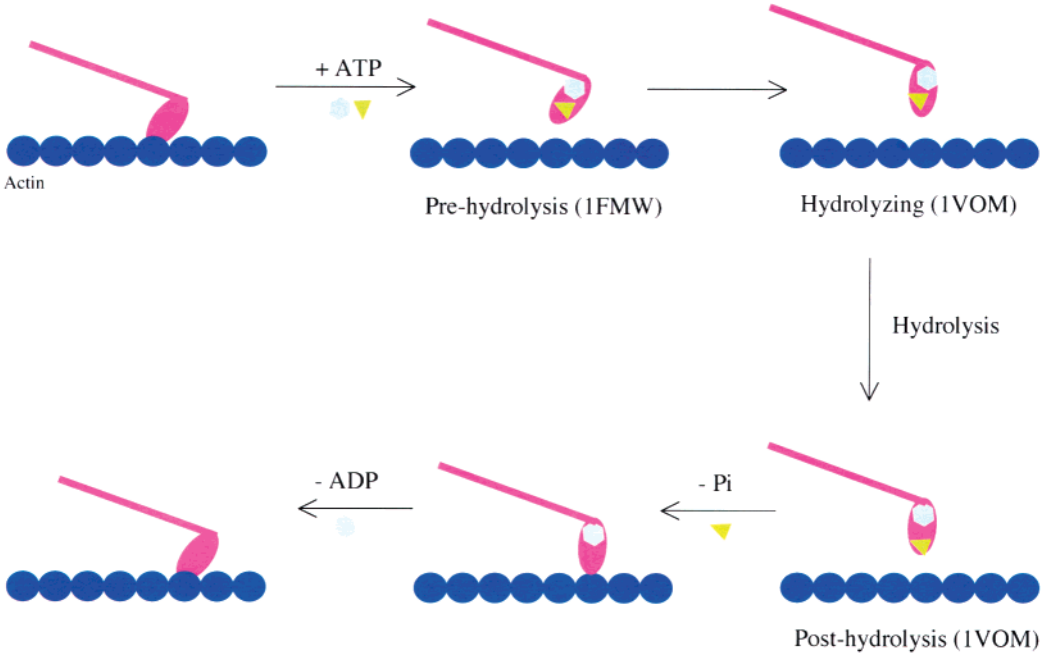

[a] Only a myosin monomer is shown.

and actin, and the detailed mechanism through which actin induces the release of inorganic phosphate and ADP.[19,25]

Concerning the ATP hydrolysis step in myosin, most information has come from high-resolution structures (<2 Å) of *Dictyostelium discoideum* myosin with different ligands and kinetic analysis of various mutants.[23,32−35,40] The motor domain is believed to adopt at least two different conformations:[19] the open state and the closed state, which was proposed to favor nucleotide binding and hydrolysis, respectively. The two active site differ mainly in a linker region that is structurally equivalent to the switch II region of G-proteins such as *Ras* p21,[41] and a key difference is the formation of a critical salt bridge between Arg238 and Glu459 in the closed form (Figure 1; see below). [The residue numbers in the *D. discoideum* myosin-II has been used throughout the manuscript.] The open state is observed when the active site is empty or bound with Mg·ATP,[40] Mg·ATP analogues (e.g., Mg·ATPγS and Mg·AMP·PNP),[42] and Mg·ADP.[42] The closed-state is observed with the active site occupied by ATP hydrolysis transition state analogues: Mg·ADP·AlF_4^- [43] and Mg·ADP·VO_4.[44] With Mg·ADP·BeF_3, both

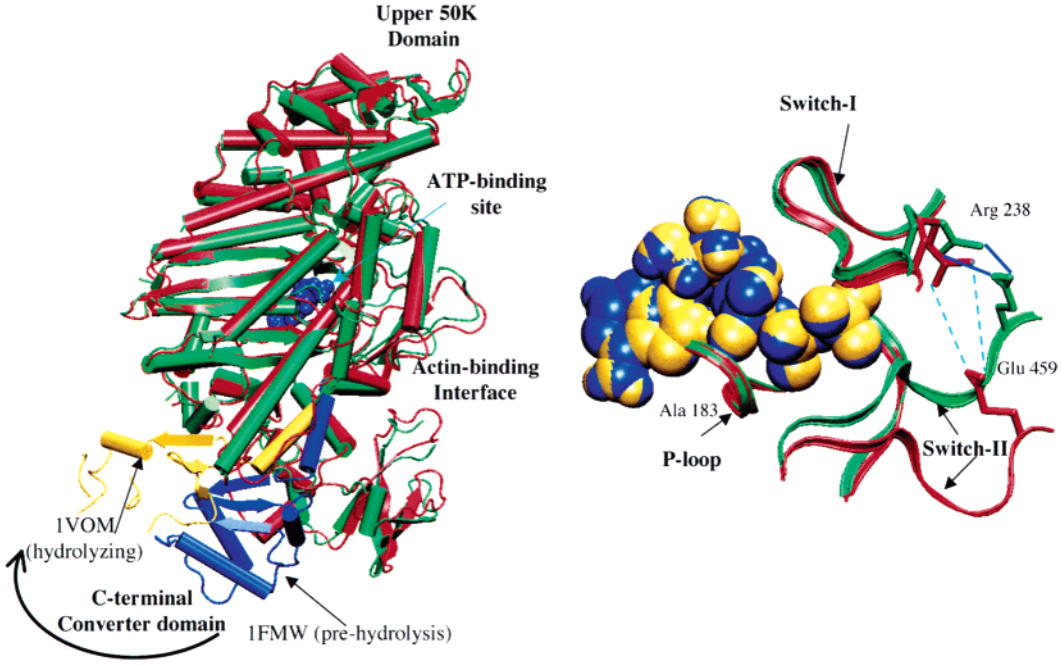

Figure 1. Difference between the prehydrolysis (1FMW) and hydrolyzing (1VOM) state of the *D. discoideum* myosin-II motor domain. (a) Superposition of the motor domain in the two states based on the backbone atoms in residue 1−650: red and blue corresponding to 1FMW; green and yellow indicating the 1VOM state. As illustrated by the arrow, the majority of the conformational difference occurs in the C terminal converter region. (b) Structural difference between the active sites of the two states, with the same color coding. The ATP molecule is shown in van der Waals representation, and the three important motifs in ATP hydrolysis are shown in ribbon. Evidently, the major changes are associated with the relative arrangements of the switch I and switch II regions, in particular the salt bridge between Arg 238 and Glu 459.

SCHEME 2. Two Associative Mechanisms for ATP Hydrolysis in Myosin[a]

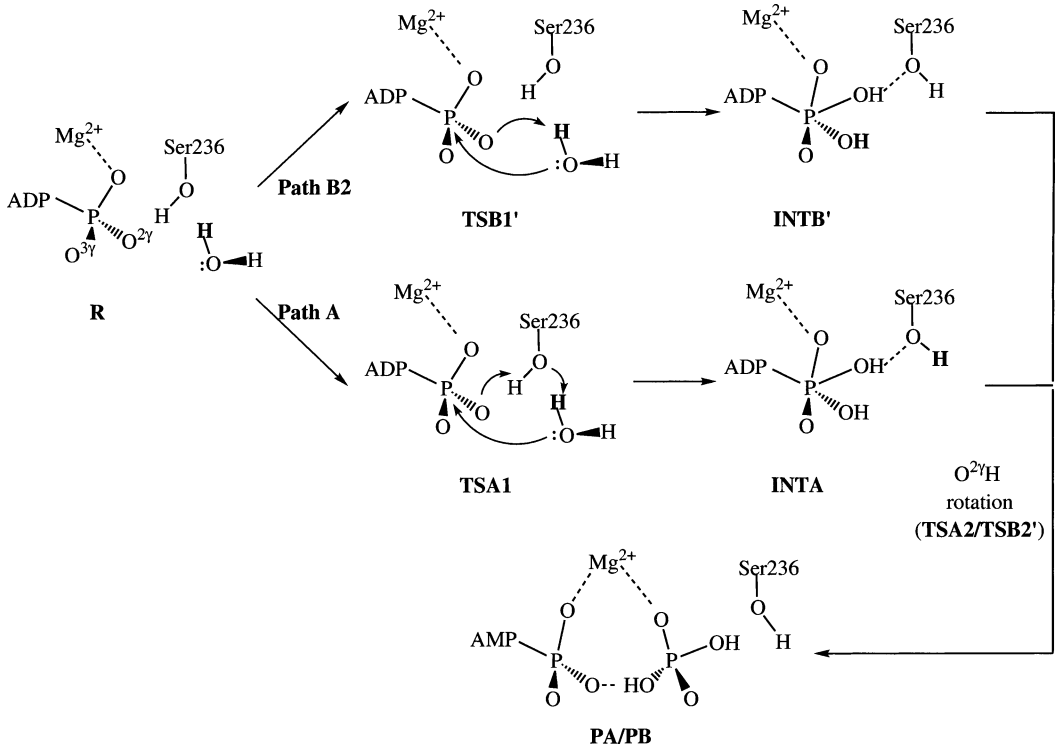

[a] In path B, a route in which the water proton is transferred directly to $O^{3\gamma}$ instead of $O^{2\gamma}$ has also been studied (path B1).

closed[19,45] and open[43] forms have been observed in X-ray crystal structures, which highlights the subtle nature of factors that control the transition between the two conformational states and the intrinsic structural flexibility of the motor domain.[15] Moreover, these structures clearly indicate that ATP binding alone is *not* sufficient to stabilize the motor domain to the conformation appropriate for hydrolysis. Since no catalytic base in the form of amino acid side chains is found within 5.5 Å of the beryllium or vanadium that mimic the γ-phosphate, it is natural to conclude that water molecule(s) in the active site is the nucleophile and the γ-phosphate serves as the general base for its own hydrolysis. A highly conserved active site Ser residue (Ser 236) was proposed to serve as a relay in this process, making the proton transfer proceed with the better stereochemistry (Scheme 2).[43,44] Although such a proton-relay mechanism has been discussed in model calculations for the *dissociative* mechanism of phosphate hydrolysis in solution,[46,47] it has not been firmly established in either the context of hydrolysis in enzymes or *associative* mechanism of phosphate hydrolysis. As a matter of fact, mutation experiments found that the S236A mutant has rather normal hydrolysis activity.[33,35] Alternative mechanisms that employs Lys 185 as the general acid that protonates the γ-phosphate of ATP has also been proposed based on recent Car-Parrinello (CP) simulations,[48] although the observation that led to this mechanism might be an artifact due to the small size of the model used in the calculations.[14] Another pair of residues that were found to be essential to hydrolysis involves Arg 238 and Glu 459, which form a salt bridge in the closed form (Figure 1b).[44] Mutation involving either one of these residues significantly impairs the hydrolysis efficiency (e.g., E459V hardly affects ATP binding, but reduces ATP hydrolysis by a factor of 10^6);[49,50] a double mutation that flips the positions of the two residues, by contrast, retained a substantial amount of ATPase activity.[49,50] These results were explained in terms of the role of the salt bridge in maintaining the appropriate water structure in the active site that favors hydrolysis, although a detailed mechanism is not available; e.g., it was proposed that the second active-site water molecule, which bridges the lytic water and Glu 459, can serve as the general base and accept one proton from the lytic water.[50] For other residues in the switch I and switch II regions, mutation experiments also provided insights into their roles in ATP binding and hydrolysis.[32−35,38] To better establish the nature of their contributions, however, a detailed analysis with energetics is of significant value.

In the present work, we have carried out both classical molecular dynamics (MD) simulations and combined quantum mechanical and molecular mechanical (QM/MM) reaction path calculations to analyze the mechanism of ATP hydrolysis in myosin with a stochastic boundary condition. Classical MD simulations were employed to investigate the structure and dynamics of active site residues and water molecules, and how these are affected by the conformation of the motor domain in different kinetic states (prehydrolysis state and hydrolysis "transition state"). The QM/MM calculations were used to qualitatively analyze two popular *associative* mechanisms for the hydrolysis of ATP, the contribution from amino acids and the dependence of hydrolysis energetics on the motor domain conformation. Computational methods and simulation details are described in section II, which is followed by the presentation of results and relevant discussions in section III. We summarize several conclusions in section IV.

II. Computational Methods

All the simulations here have been set up using the stochastic boundary conditions (Figure 2).[51−53] A water sphere of 18 Å is centered on the active site of myosin-II motor domain, and the system is divided into the reaction (<16 Å), buffer (16−18 Å) and reservoir zone (>18 Å). Atoms in the reservoir zone were excluded in the simulation, and those in the buffer zone were subject to harmonic constraints and random force following the

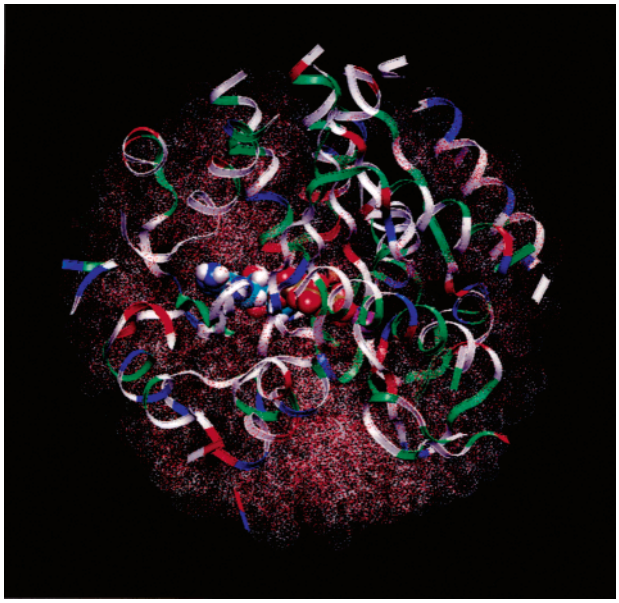

Figure 2. Stochastic boundary setup for the present simulations. The protein atoms areshown in the ribbon format, and are color-coded according to the type of the amino acids (white, nonpolar; green, polar; blue, acidic; red, basic). The ATP molecule and the magnesium ion are shown in van der Waals representations. The solvent molecules are shown as dots.

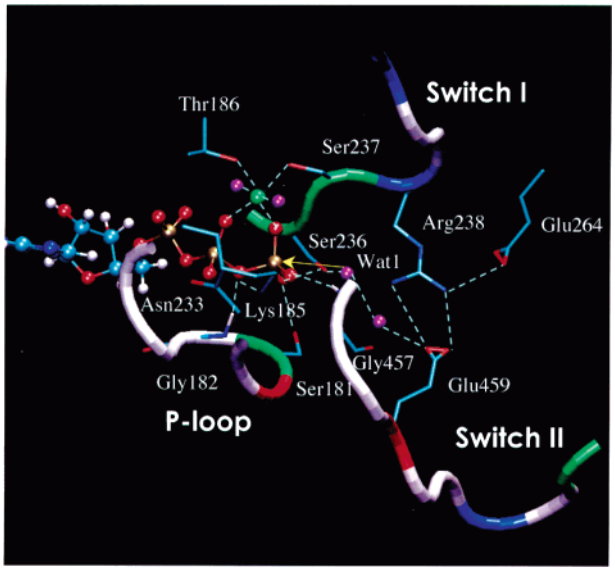

Figure 3. Active site structure of the *D. discoideum* myosin-II motor domain in the hydrolyzing state (PDB code 1VOM). The loops indicate the three important structural motifs (the P-loop, switch I, and switch II), which are commonly found in proteins involve nucleotide binding and hydrolysis; they are color-coded as in Figure 2. Part of the ATP molecule, the magnesium ion and several important water molecules are shown in the CPK format, while the side chains of several important residues are shown in the line form. Among those, the shown moiety of ATP, the magnesium ion and its ligands (Thr 186, Ser 237, and two water molecules), the lytic water (Wat 1) and Ser 236 were treated with QM in the QM/MM calculations (see text).

Langevian equation. In the classical MD simulations, the integration time step was 1 fs, and all bonds involving hydrogens are constrained using SHAKE.[54] The temperature of the system was maintained at 300 K using the mixed molecular dynamics/Langevian dynamics scheme unique to the stochastic boundary simulations.[51−53] All classical simulations were performed using the CHARMM program[55] with the CHARMM 22 force field[56] for the protein atoms and ATP/ADP·Pi.

In the QM/MM calculations,[10−13] the QM region included the tri-phosphate and part of the ribose group of ATP, the catalytic water molecule(s), the Mg^{2+} ion and all its ligands (Thr 186 and Ser 237 and two water molecules) as well as the conserved Ser 236 (Figure 3). In the current work, ATP was assumed to be fully deprotonated (i.e., −4 charge) and the ligands of Mg^{2+} were assumed to remain protonated; all other titritable groups were kept in their normal protonation states (i.e., Lys, Arg were protonated, Asp, Glu were deprotonated), which are consistent with a simple estimate of pK_a's using Poisson−Boltzmann approach.[57] All other atoms, including the charged (e.g., Lys 185) and polar side chains (e.g., Asn 233) as well as main chain groups (e.g., Gly 457) that are close to the reacting atoms (Figure 3), were treated with the CHARMM 22 force field;[56] this makes it convenient to analyze the qualitative contributions from protein residues to the ATP hydrolysis energetics. A Poisson−Boltzmann (PB) charge-scaling scheme[58] was introduced to account for solvent shielding in addition to that from the explicit water molecules in the model. The algorithm makes use of several PB calculations to determine a set of scaling factors to reduce the partial charges of charged side chains in the QM/MM calculations so as to avoid artifactual structural changes.[59] Link atoms were introduced to saturate the valence of the QM boundary atoms; the link atoms interact with the MM atoms, except the "link host" MM atom (e.g., the Cα atoms in this case), through electrostatic terms; no van der Waals interactions are included. This scheme has been shown to be a satisfactory way to treat the QM/MM interface, particularly when the charges of the atom in the neighborhood of the link atom are small, which is true in the present case.[60] The QM method used in geometry optimization and reaction path calculations is HF[61]/3-21+G,[62,63] and B3LYP[64−66]/6-31+G(d,p)[67,68] was used in single point energy calculations; test calculations indicate that such a scheme gave very similar energetics compared to using B3LYP/6-31+G as the QM method in geometry optimizations. The van der Waals parameters used for QM atoms are the standard CHARMM parameters. Benchmark calculations for phosphate hydrolysis reactions in the vacuum and solution indicate that B3LYP/6-31+G(d,p) energetics are sufficient for our purpose of comparing various mechanisms.

In the reaction path calculations, an initial guess was first generated by adiabatic mapping[69] calculations employing approximate reaction coordinates, such as the antisymmetric stretch involving the proton donor, the proton and the proton acceptor atoms.[59] This path was then further refined using the conjugate peak refinement[70] approach in CHARMM to obtain more accurate information about the relevant saddle points. All the protein atoms were allowed to move in the reaction path calculations, although their thermal fluctuations are clearly not included. Therefore, the current reaction path results should be taken as qualitative, although previous experience suggests that this type of calculations is capable of providing mechanistic insights.[59,71,72] Calculations employing a more realistic treatment of protein motions and structural response to the chemical event,[14,73,74] which necessarily involves less expensive QM methods,[75−77] are in progress and will be reported in the near future.

As to the starting atomic coordinates, two high-resolution X-ray structures from *D. discoideum* were used. They were determined with Mg·ATP (PDB code 1FMW[40]) and Mg·ADP·vanadate (PDB code 1VOM[44]) as the ligands, respectively, and were believed to correspond to the prehydrolysis and hydrolyzing kinetic states, respectively.[19,23] The starting structures for

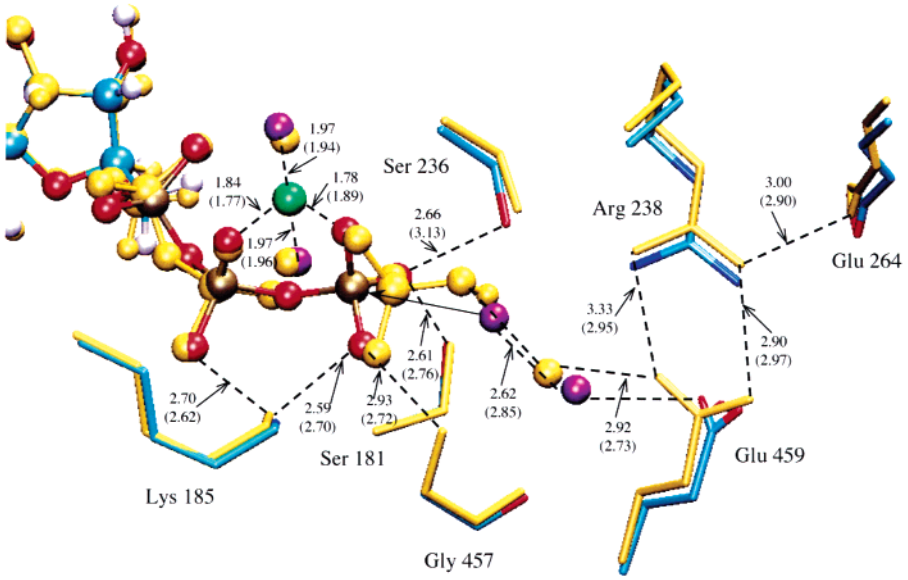

Figure 4. Overlay of the averaged positions for part of ATP/ADP·Pi and several aminoacids in the active site from 500 ps classical molecular dynamics simulations for 1VOM. The color-coded ones are from ATP simulations, while the yellow ones are from the MD simulation in which ATP was replaced by ADP·Pi. Note that there are essentially no major structural changes during the 500 ps of simulations. Key distances are given in angstroms; those with and without parentheses are for the ATP and ADP·Pi simulations, respectively.

QM/MM calculations are the minimized X-ray structures, rather than those from classical MD simulations; this is based on the consideration that structures from classical MD simulations are usually fairly different from the X-ray data, which are not appropriate for QM/MM calculations unless free energy quantities are calculated.[74] By comparing simulation results for these two structures, we are able to explore the connection between ATP hydrolysis and conformational properties of the motor domain in myosin. In the 1VOM simulations, the ADP·vanadate was replaced by ATP or ADP·Pi.

III. Results

In this section, we first describe the features of the myosin active site from classical molecular dynamics simulations, and then move on to the combined QM/MM analysis of the catalytic and regulatory mechanism of ATP hydrolysis.

III.1. Active Site Structure and Dynamics of Myosin in the Hydrolyzing (1VOM) and Prehydrolysis (1FMW) States. Since MD simulations have been reported on the myosin motor domain before,[48,78] we will only describe the results briefly and focus on the differences between the prehydrolysis (1FMW) and hydrolyzing (1VOM) states.

With the 1VOM structure, the active site is stable in the 500 ps of MD simulations with either ATP or ADP·Pi bound; the same trend was also found in alchemy free energy simulations that last for several nanoseconds (Li et al., to be submitted). This includes not only the critical interactions between ATP and the surrounding amino acids (Figure 4) but also the two active-site water molecules resolved in the X-ray structure.[44] As shown in Figures 4 and 5c,d, these water molecules form a hydrogen-bonding network that connects the γ-phosphate in ATP and Glu 459; the latter is in the switch II region and is stabilized by a salt bridge interaction with Arg 238 in the switch I region. Because of such a network, the water closer to the γ-phosphate is in a favorable position for a nucleophilic attack; as shown in Figure 5a,b, the $O^W-P_\gamma{}^{ATP}$ distance is stable around 3.2 Å, and the $O^W-P_\gamma{}^{ATP}-O_{3\beta}{}^{ATP}$ angle undergoes only mild fluctuations about 155°.

The active site undergoes small structural changes when the ATP molecule was replaced by ADP·Pi. As shown in Figure 4, the averaged structure from the two sets of MD simulations superimpose very well, such as the positions of Lys 185, Ser 236 and Gly 457. The salt bridge between the switch I and switch II regions also remained intact. The small structural perturbation associated with replacing ATP by ADP·Pi observed here led us to believe that reaction path calculations using a QM/MM potential is a meaningful first step to explore the energetics and mechanism of ATP hydrolysis in myosin (section III.2.3).

The prehydrolysis state (1FMW) has a very similar overall structure compared to the hydrolyzing state (1VOM); the first 650 amino acids can be aligned to have only a 2.4 Å RMS difference for the backbone atoms, while the C-terminal converter domain undergoes a large swinging displacement (Figure 1a).[15,40] In the present study, we only focus on the active site region, for which a key difference is the relative arrangement of the switch I and switch II regions (Figure 1b). In 1FMW, the salt bridge between Glu 459 and Arg 238 is broken, and the mainchain of Gly 457 can no longer stabilize the γ-phosphate of ATP. These trends remained during the MD simulations for 1FMW. As shown in Figure 6, Arg 238, Glu 459, and Gly 457 are among the ones with the most significantly different average positions between 1VOM and 1FMW simulations. In 1FMW, Arg 238 is substantially closer (~0.4 Å) to the γ-phosphate, and Glu 459 and Gly 457 are further away from Arg 238 and ATP, respectively. Because of these structural changes, the water distributions in the active site are also different in 1FMW and 1VOM. The trapped water molecules underwent significantly larger fluctuations in 1FMW (Figure 5c,d), and orient themselves differently. As shown in Figure 5a,b for the two water molecules close to the γ-phosphate, the $O^w-P_\gamma{}^{ATP}$ distances vary from 3 Å to 4.2 Å, and the $O^W-P_\gamma{}^{ATP}-O_{3\beta}{}^{ATP}$ angles vary from 100 to 150°. Therefore, the water molecules in 1FMW are not in as favorable positions as the ones in 1VOM for nucleophilic in-line-attacks. The energetical consequences of these differences will be revealed by the subsequent QM/MM analysis (Section III.3).

Similar to 1VOM, the active site underwent small structural changes when the ATP was replaced by ADP·Pi during the 500 ps of MD simulations (not shown).

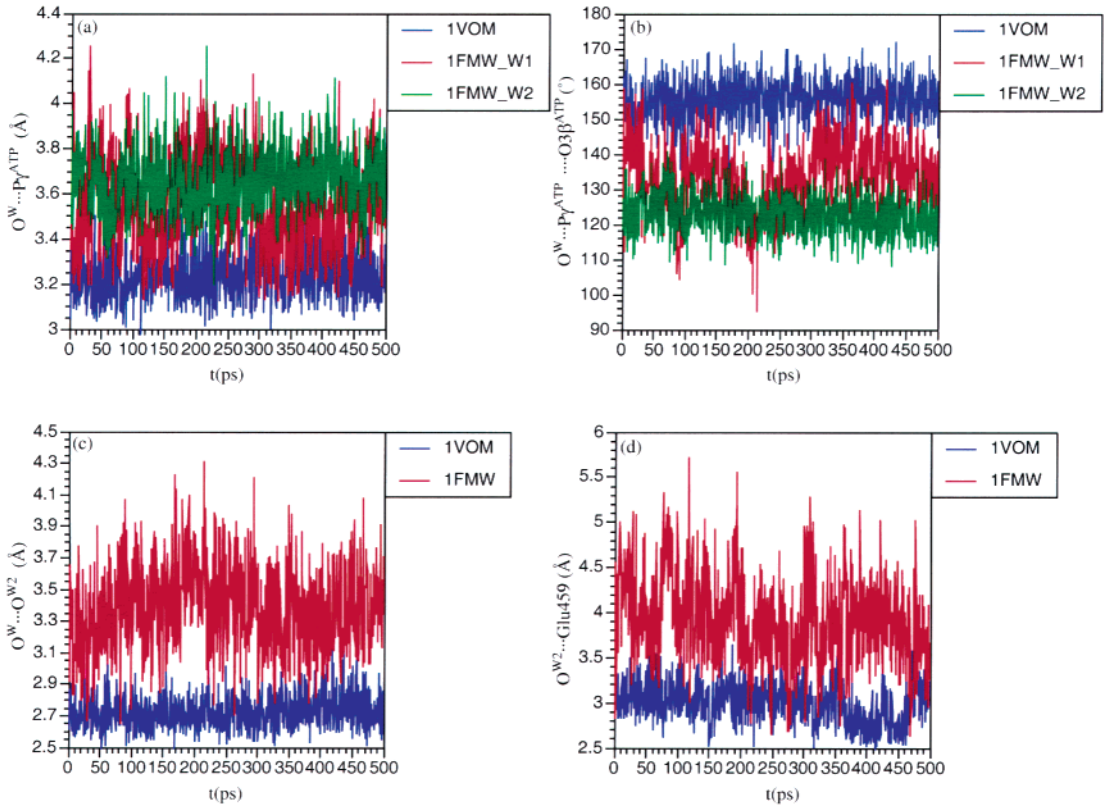

Figure 5. Instantaneous values of several key geometrical parameters that characterize the water structure in the active site during MD simulations. For both 1FMW and 1VOM simulations, the active site is occupied by ATP. The geometrical parameters include (a) the distance between the oxygen in lytic water molecule(s) and Pγ of ATP, (b) the angle between the oxygen in lytic water molecule(s) and Pγ−O3β of ATP, (c) the distance between the oxygen atoms in the two water molecules close to the γ-phosphate, and (d) the minimal distance between Glu 459 and the oxygen atoms in the two water molecules close to the γ-phosphate. Note the larger fluctuations and deviation from ideal in-line attack orientations associated with the 1FMW simulations.

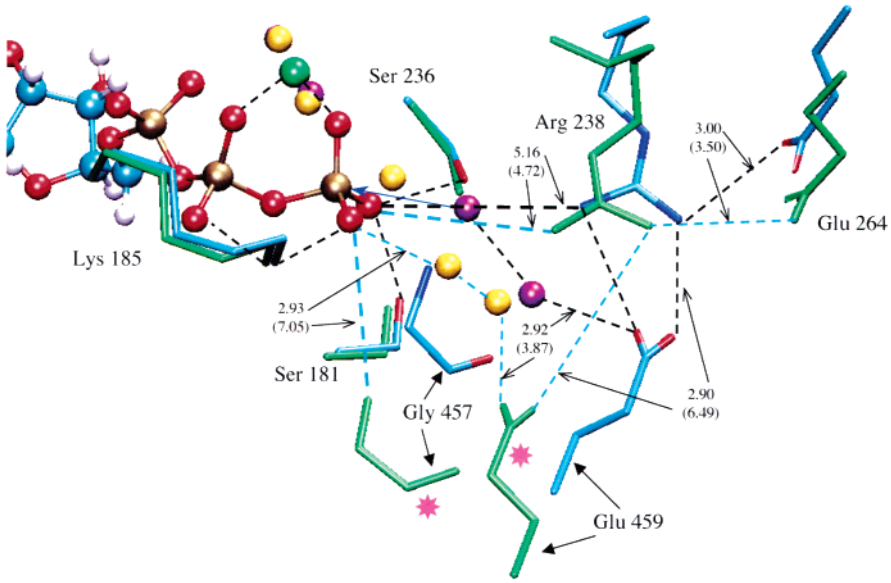

Figure 6. Similar to Figure 4, but for 1FMW and 1VOM simulations with ATP as the ligand. Note the significantly differences in the switch II region. Only the distances that are very different in the two sets of simulations are given.

III.2. Energetics and Mechaisms of ATP Hydrolysis in the Hydrolyzing Structure (1VOM). As discussed in the Introduction, at least two possible reaction schemes have been proposed for ATP hydrolysis in myosin (Scheme 2); one mechanism involves a direct proton transfer from the attacking water to the γ-phosphate (path B), and the other involves Ser 236 as the proton relay (path A). According to the QM/MM reaction path results summarized in Figure 7, path A has a lower rate-limiting activation barrier and therefore is likely to be the favorable pathway in wild-type myosin; the energetics associated with path B depend on which γ-oxygen gets protonated, and the lower energy route has a rate-limiting barrier only ∼4 kcal/mol higher than path A.

In path A, the lytic water molecule first transfers one of its proton to the hydroxyl oxygen in Ser 236, which in turn transfers its hydroxyl proton to the γ-phosphate. Only one transition state

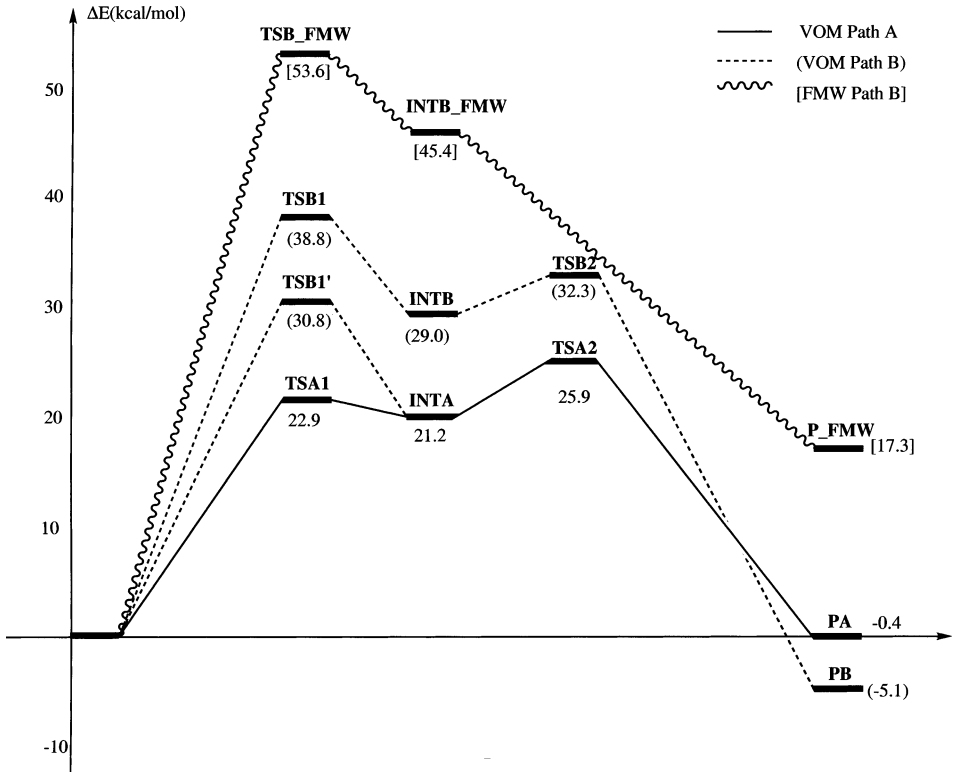

Figure 7. Schematic potential energy diagrams associated with the several hydrolysis pathways studied here with QM/MM reaction path calculations. For the definition of path A and B, see Scheme 2.

was found for these two proton transfers. In **TSA1** (Figure 8), the water proton is shared between the donor (O^w) and the acceptor atoms (O^{S236}), while the hydroxyl proton in Ser 236 has nearly completed the transfer to the γ-phosphate oxygen ($O^{2\gamma}$). The distance between the lytic water and P^γ has decreased from 2.852 Å in the reactant (**R**) to 1.916 Å in **TSA1**, and the distance between P^γ and the bridging β oxygen ($O^{3\beta}$) correspondingly has increased from 1.709 Å to 1.805 Å. In the pentacoordinated intermediate, **INTA**, the O^w-P^γ distance is further shortened to 1.794 Å and the $P^\gamma-O^{3\beta}$ distance is lengthened to be 1.855 Å. To lead to the final hydrolysis products, a rotation of the newly formed $O^{2\gamma}$-H group has to occur (**TSA2**), which induces the break of the bond between P^γ and $O^{3\beta}$. In the final product, **PA**, the $O^{2\gamma}-H$ interacts with $O^{3\beta}$ through a very short hydrogen bond, in which the $H\cdots O^{3\beta}$ is only 1.319 Å. Although this short distance could be an artifact of the HF/3-21+G method used in geometry optimization, it is reasonable to expect a strong interaction between the negatively charged ADP and the OH group in Pi. Despite the stabilizing interactions from positively charged and polar groups in the active site, such as Mg^{2+}, Lys 185, and the main chain of Gly 457, there is substantial repulsion between the negatively charged ADP and Pi. As a result, the hydrolysis products are nearly the same in energy compared to ATP (−0.4 kcal/mol, Figure 7) in the myosin motor domain, rather than being much more stable than ATP as reflected by the large exothermicity associated with the hydrolysis in solution. In the entire hydrolysis process, the second transition state is the highest in energy, which is only 3 kcal/mol higher compared to **TSA1**; the present calculations are not sufficiently accurate to rule out the possibility that **TSA1** is rate-limiting. The pentacoordinated intermediate, **INTA**, is only marginally stable as implied by the small barriers that separate it from the reactant and product states, and it is 21.2 kcal/mol higher in energy than **R**. The high energy nature of the intermediate makes it in general difficult to capture in structural studies, and the first pentavalent intermediate in a phosphoryl transfer reaction has only been reported very recently.[79]

In path B, two possible routes can be followed depending on to which γ-oxygen is the water proton transferred (Scheme 2). With the water geometry in **R** (Figure 8), the $O^{2\gamma}$ is "protected" by the hydrogen-bonding interaction with Ser 236, and the lytic water proton is oriented toward $O^{3\gamma}$. In the corresponding transition state (**TSB1**), the O^w-P^γ distance is longer than that in **TSA1**, which are 1.996 and 1.916 Å, respectively; the $P^\gamma-O^{3\beta}$ distances are 1.744 and 1.805 Å, respectively, which are also consistent with the earlier nature for **TSB1**. The proton transfer occurs in a four-membered ring arrangement, where the $P^\gamma-O^w-H$ angle is only 69.9°, which is not optimal from a stereochemistry point of view. Indeed, the barrier associated with **TSB1** is substantially higher than **TSA1** by nearly 16 kcal/mol, although the difference does not necessarily come entirely from the four-membered ring arrangement in **TSB1**. For example, due to the interaction with the lytic water in **TSB1**, $O^{3\gamma}$ loses interaction with the mainchain of Gly 457 and a water molecule trapped in the active site, which are present in **TSA1**; the relevant hydrogen bonding distances are 2.05, >3 Å in **TSB1** compared to 1.73 and 1.70 Å in **TSA1**. The pentavalent intermediate along path B1 (**INTB**) is slightly more compact than **INTA** in terms of the O^w-P^γ and $P^\gamma-O^{3\beta}$ distances by approximately 0.05 and 0.03 Å, respectively. Because of the different protonation patterns of γ-oxygens, **INTB** is less stable than **INTA** by nearly 8 kcal/mol. In addition to the differences in the interaction between $O^{3\gamma}$ with Gly 457 and active water as already observed in the transition states, protonation of $O^{3\gamma}$ in **INTB** weakens the interaction with a charged group, Lys 185, while the protonation of $O^{2\gamma}$ in **INTA** weakens interactions with neutral groups such as Ser 236 and Ser 181. The subsequent isomerization of the $O^{3\gamma}H$ group in **TSB2** takes a similar amount of energy (~3 kcal/mol) as in path A, and the final hydrolysis products are slightly more stable than the reactant state. Interestingly, the final products have ADP protonated and the

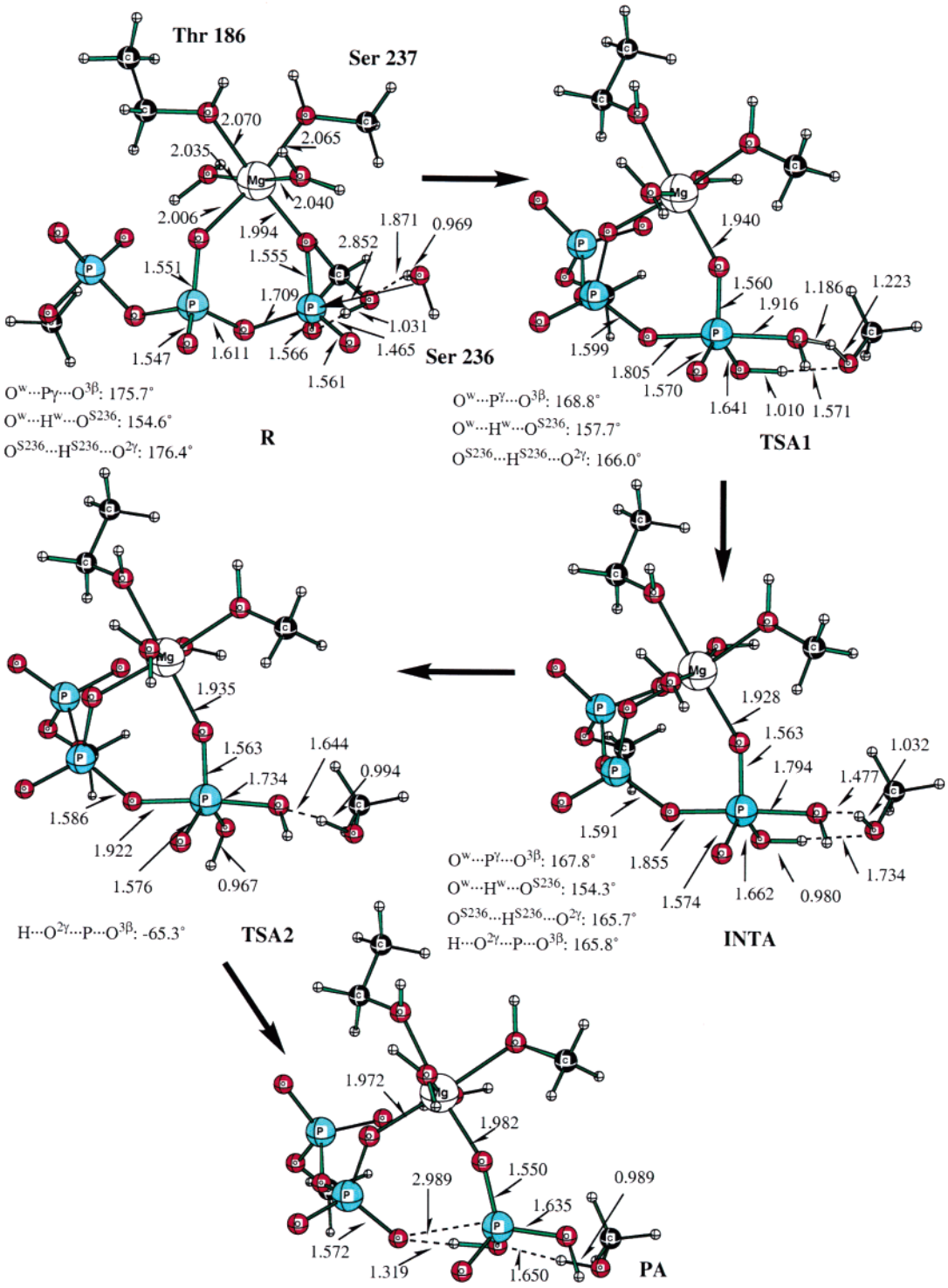

Figure 8. Geometries for the reacting groups during the hydrolysis reaction following path A, when the motor domain is in the hydrolyzing state (1VOM). The geometries were obtained from HF/3-21+G/CHARMM reaction path calculations (see section II); distances are given in angstroms, angle and dihedral angles are given in degrees. Note that the protein environment has been included in the framework of the stochastic boundary condition (Figure 2 and section II of main text), although only the QM atoms are shown here.

inorganic phosphate monprotonated, although the hydrogen bond between the two is very short with a distance between the hydrogen and the acceptor atom ($O^{3\gamma}$) of 1.377 Å.

Alternatively, path B can proceed through a proton transfer from the lytic water to $O^{2\gamma}$ (path B2). To do so, however, the reactant geometry has to change to allow the direct interaction between the water proton and $O^{2\gamma}$. By rearranging orientations of the protons in the lytic water and Ser 236, we obtained structure **R′** (Figure 10). The lytic water in **R′** is directly hydrogen bonded to $O^{2\gamma}$ and Ser 236 is hydrogen bonded to the oxygen in the lytic water with rather short hydrogen bond distances around 1.5 Å. The distance between the lytic water and P^{γ} is a bit longer, 3.261 Å, than that in **R** (2.852 Å), and the angle $O^{w}-P^{\gamma}-O^{3\beta}$ is less linear (150.2° vs 175.7° in **R**). In the corresponding transition state, **TSB1′**, the $O^{w}-P^{\gamma}$ distance is also longer, which is 2.250 Å compared to 1.996 Å in **TSB1**. The interesting difference with **TSB1** is that **TSB1′** appears to be later in nature based on the observation that the water proton has almost completed the transfer to $O^{2\gamma}$; the $H^{w}-O^{w}$ and $H^{w}-O^{2\gamma}$ distances are 1.435 and 1.043 Å, respectively. Following

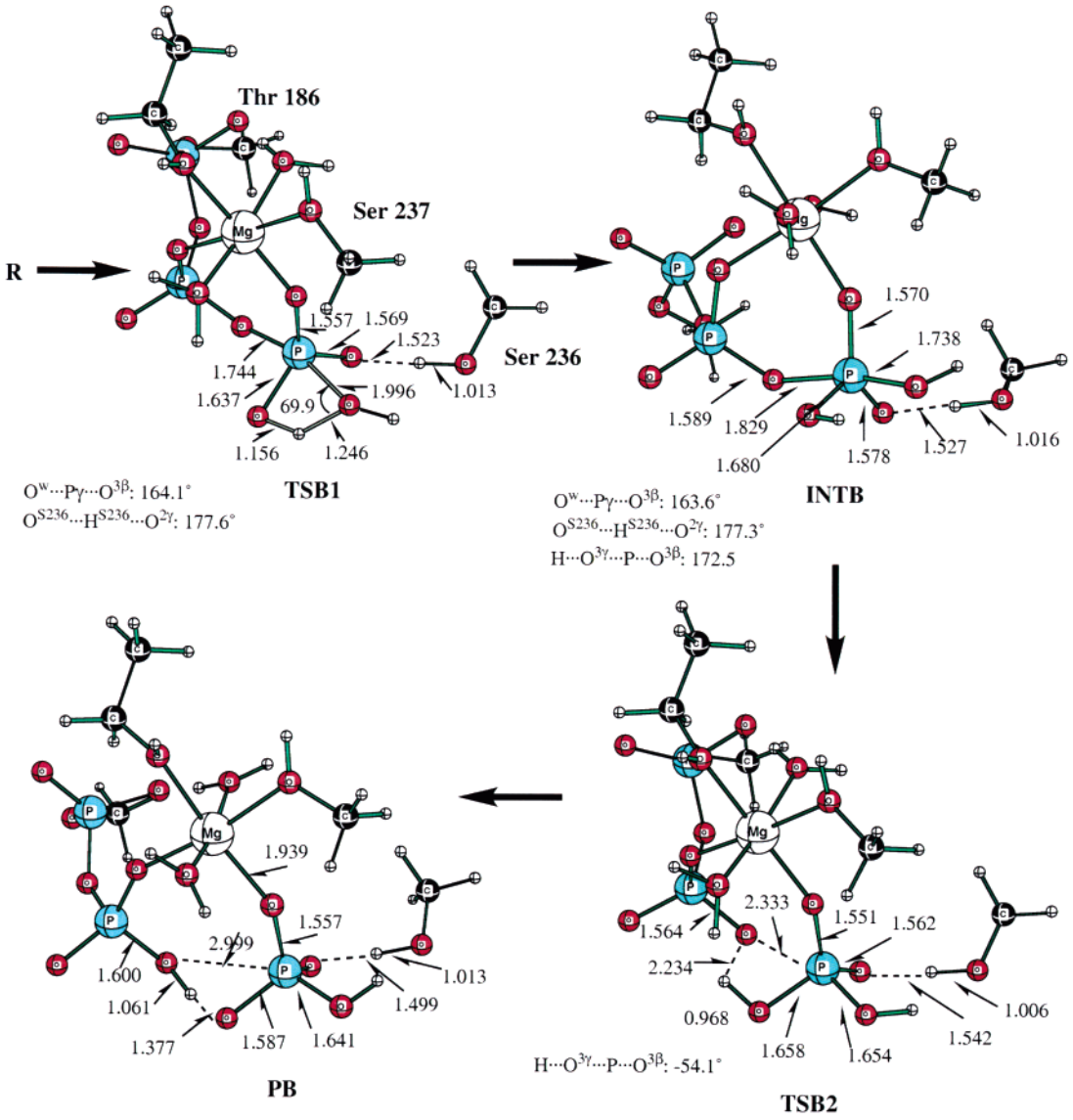

Figure 9. Similar to Figure 8, but for the structures involved in path B1.

TSB1′, the pentavalent intermediate is essentially the same as **INTA**, and therefore the rest steps have the same energetics as discussed for path A. **TSB1′** is lower than **TSB1** by nearly 8 kcal/mol because it is less favorable to protonate $O^{3\gamma}$ as in the latter, which leads to weaker interactions with the mainchain of Gly 457 and an active site water molecule. Nevertheless, **TSB1′** is still higher than **TSA2** by ~5 kcal/mol, which is about the uncertainty of the present QM/MM reaction path analysis. Therefore, although path A is likely to be the dominant path in wild-type myosin, we cannot exclude the possibility that path B2 also contributes (see below).

To further understand qualitative contributions from various residues, perturbation analysis[59,72,80] has been carried out on critical QM/MM energetics. For path A, it is seen that the same cluster of residues contribute to different steps of the hydrolysis, such as Ser 181, Lys 185, Asn 233, Arg 238, and Glu 459; several Gly residues also contribute significantly due to their main chain interactions. The sign of their contributions, however, change depending on the nature of the reaction steps. Take Lys 185, for example, it favors the formation of **INTA** and the final product **P** over the reactant state by more than 6 kcal/mol, while it contributes unfavorably to the barrier **TSA2** (Figure 11). Apparently, as $O^{2\gamma}$ gets protonated in **INTA** and **P**, the negative charge distribution is more shifted toward $O^{3\gamma}$, which results in a stronger interaction with Lys 185. The critical role of Lys 185 is consistent with the previous mutation study, which showed that the Lys185Q mutation abolished the ATPase activity.[33] A neutral residue, Ser 181, which interacts with $O^{2\gamma}$ in the reactant state (Figure 1), significantly destabilize **INTA** and **PA** over **R** due to the protonation of $O^{2\gamma}$ in the former two states. The fact that Ser 181 is not required for catalysis is qualitatively consistent with the mutation result that Ser181A/Ser181T showed nearly normal ATPase activity.[33] Two glycine residues in the P-loop region, Gly 182 and Gly 184, were found to contribute favorably (~2 kcal/mol) to **TSA1** and **INTA**, while Gly 457 in the switch II region significantly favored the formation of the hydrolysis product by ~3 kcal/mol. The contribution from Gly 457 is consistent with the previous mutagenesis result that mutating Gly 457 into Ala reduced the hydrolysis activity by $\sim 10^5$ fold.[32,34] For the two Asn residues in the active site, Asn 233 and Asn 235, their contributions were found to be small for the rate-limiting step in path A (Figure 11). This observation is consistent with the experimental data that Asn235A and Asn235I had near-normal ATPase activity;[33,35] Asn233 was believed to be more important for ATP binding because Asn233A did not bind ATP.[33,35] Since the perturbation analysis was made with a limited number of configurations from QM/MM reaction path calculations, we

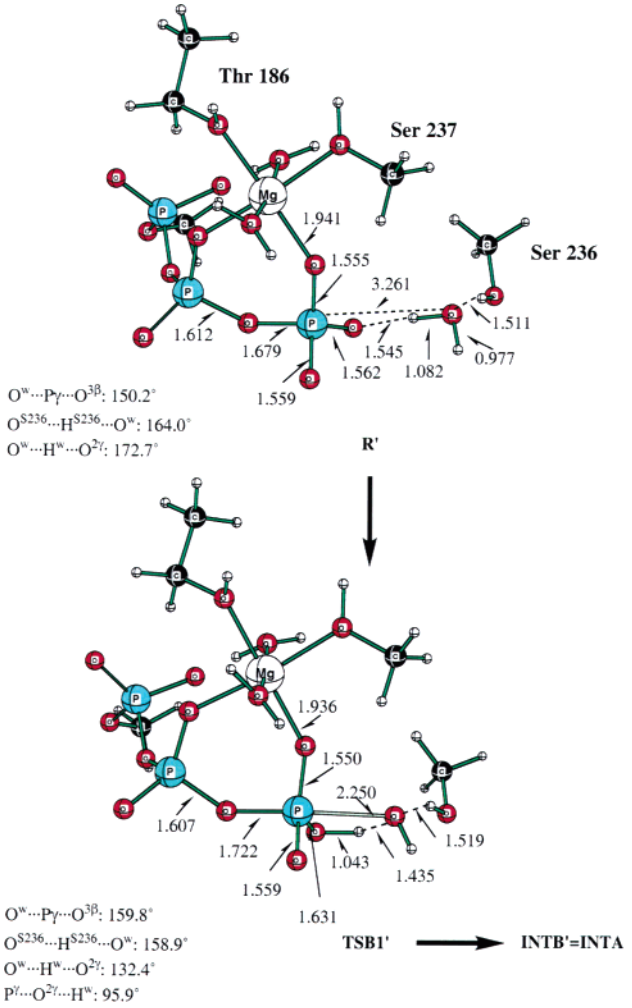

Figure 10. Similar to Figure 8, but for the structures involved in path B2.

emphasize that the results should be taken as approximate, especially for those have small values (<2 kcal/mol). For example, the perturbation results indicate that D454 and S456 make small unfavorable contributions to the hydrolysis intermediate and product formations (Figure 11); experimentally, S456A and S456L mutants showed nearly the same ATPase activity as the wild type,[34,38]while mutating D454 into Ala decreased the hydrolysis rate by ∼2000-fold.[32] More conformational sampling and calculations with the actual mutations need to be performed in the future for a better understanding of contributions from these residues.

Since the major difference between path A and B is in the first transition state, only the perturbation results for **R**(**R′**) → **TSB1** (**TSB1′**) are shown in Figure 12. Because $O^{3\gamma}$ and $O^{2\gamma}$ are protonated in **TSB1** and **TSB1′**, respectively, it is expected that Ser 181 disfavors **TSB1′** while it has a negligible effect on **TSB1**, which were confirmed by the perturbation analysis (Figure 12). For the similar reason, we expect that Lys 185 has different effects on the two routes of path B. Interestingly, the contribution from Lys 185 was found to be rather small in the transition states, although the expected effect did show up clearly in the intermediates (not shown). This indicates that charge redistribution among the γ-oxygen atoms has not yet occurred in the transition states, and the weaker interactions between $O^{3\gamma}$ and mainchain of Gly 457 and the active site water in **TSB1** are the major causes for the higher barrier compared to **TSB1′**. In **TSB1**, we note that Glu 459 contributes favorably to the barrier with a magnitude larger than that in **TSA**, while Asn 233 contributes unfavorably due to the weakened interaction with $O^{2\gamma}$. Overall, the perturbation analysis did not indicate any extra destabilizing effect from the protein that significantly disfavors path B2 over path A. Therefore, the different barrier heights associated with the two mechanisms are mainly determined by the "intrinsic" nature of the direct proton transfer (path B2) vs relayed proton transfer (path A).

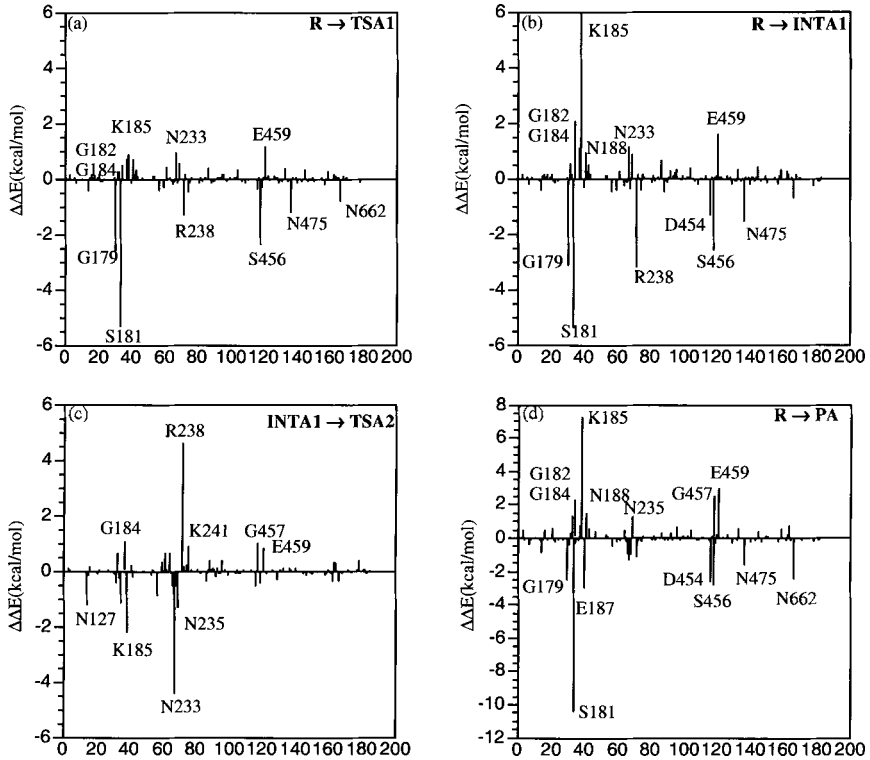

Figure 11. Results from perturbation analysis of the QM/MM energetics associated with selected steps in path A. Positive (negative) values indicate favorable (unfavorable) contributions.

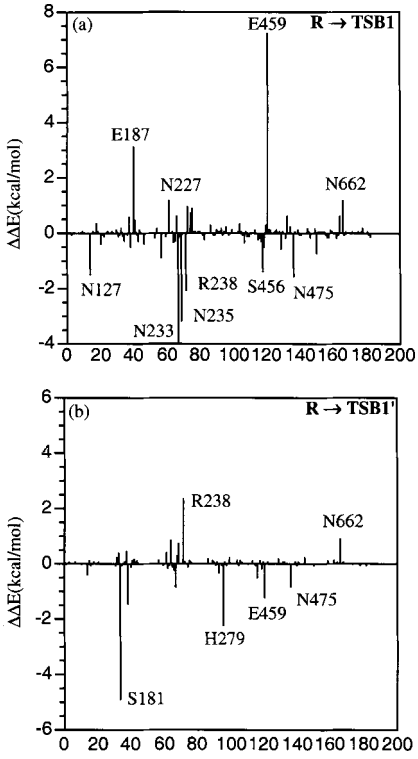

Figure 12. 12. Similar to Figure 11, but for the initial transition states in path B1 and B2.

III.3. Energetics of ATP Hydrolysis in the Prehydrolysis Structure (1FMW). With the 1FMW structure of the motor domain, QM/MM minimizations led to structures like **R_FMW** in Figure 13. Similar to the trend found in classical MD simulations discussed above, the difference in the active site of 1FMW led to different water positions. In **R_FMW**, which is one of the representative reactant state structures, the water molecule nearby the γ-phosphate is far from the ideal in-line attack orientation; several other QM/MM minimizations with different initial geometries also led to the similar arrangement. The O^w-P^γ distance is 4.021 Å, and the $O^w-P^\gamma-O^{3\beta}$ angle is 118.1°, which can be compared to the values of 2.852 (3.261) Å and 175.7° (150.2°) in **R** (**R′**). The lytic water is no longer in close contact with Ser 236, and therefore the only possible mechanism to follow is path B. In **TSB_FMW**, the key geometrical parameters of reacting species are quite similar to those in **TSB1**, such as the O^w-P^γ distance and the four-membered ring motif (Figure 13, 9); the same trend holds for the pentacoordinated intermediate and the final product. For example, in **P_FMW**, the ADP is also protonated and the inorganic phosphate is monoprotonated, as in **PB**. The energetics, however, are very different in the two cases. In 1FMW, the first barrier is 53.6 kcal/mol above **R_FMW**, which is nearly 15 kcal/mol above even the higher barrier (**TSB1**) in the path B of 1VOM; the intermediate in 1FMW is also very high in energy, 45.4 kcal/mol, and the hydrolysis products are 17.3 kcal/mol higher than the reactant state **R_FMW**.

By comparing results from perturbation analysis for 1FMW (Figure 14) and 1VOM (Figures 11−12), one can see that the two residues that stand out as destabilizing **TS1_FMW** and **P_FMW** are Arg 238 and Ser 456, which are in the switch I and switch II regions, respectively (Figure 1). Apparently, these two residues interact more favorably with the ATP state than with other chemical states, and their contributions are more distinct in 1FMW because they are closer to ATP in 1FMW than in the 1VOM structure (Figure 3). In addition, the favorable interaction from the mainchain of another switch II residue, Gly 457, is absent in 1FMW because Gly 457 is far from the γ-phosphate (Figure 4). Nevertheless, the difference in the direct protein contributions between the two sets of structures is smaller than the difference in the calculated energetics. For example, the sum of significant unfavorable contributions (absolute value >1 kcal/mol) to the hydrolysis exothermicity is ∼28 and 25 kcal/mol for 1FMW and 1VOM, respectively, while that for favorable contributions is ∼18 and ∼20 kcal/mol, respectively; these differences are smaller than the computed difference in hydrolysis exothermicity of ∼17 kcal/mol. Although considering the highly qualitative nature of the perturbation analysis, this observation suggests that an essential part of the conformational dependence of hydrolysis energetics has to come from the orientation of water molecules in the reactant state, which in turn is controlled by the protein structural feature in the active site, such as the salt bridge between the switch I and switch II regions (Arg 238−Glu 459).

III. 4. Discussions: Catalytic and Regulation Mechanisms of ATP Hydrolysis in Myosin. ATP hydrolysis is a key reaction in bioenergetics, and regulation of the hydrolysis reaction by protein conformations is the key element of the mechanochemical coupling. Providing atomic details about the catalysis and regulation of ATP hydrolysis is the major challenge in understanding energy transductions in biological systems. In the present work, we have made the first step toward this goal with classical molecular dynamics and combined QM/MM reaction path calculations for myosin-II.

On the ATP hydrolysis mechanism, two possible *associative* mechanisms have been studied (Scheme 2). Both involve an active site water molecule as the nucleophile and the phosphate itself as the general base; the two mechanisms differ in the way that the water proton gets transferred to the γ-phosphate. It was found that the energetics of path B, which involves a direct proton transfer from the lytic water to the γ-phosphate, depend on whether $O^{2\gamma}$ or $O^{3\gamma}$ is the proton acceptor. The route that protonates $O^{2\gamma}$ (path B2) is lower in energy, because the mainchain of Gly 457 and an active site water can further stabilize $O^{3\gamma}$ as the charge on the γ-phosphate reorganizes during the proton transfer; Lys 185 also plays a role although the effect was found to be small at the transition state and more notable in the intermediate. Nevertheless, both routes in path B have barriers higher than that in path A, where Ser 236, a conserved residue, serves as the proton relay group. Perturbation analysis indicated that protein residues do not have particularly destabilizing effects in path B2, and therefore, the difference between path A and B is largely due to the stereochemical factors intrinsic to direct proton transfers and OH relayed proton transfers. It has been demonstrated in previous studies[46,47] that a relayed proton transfer is energetically more favorable than a direct proton transfer because the latter involves a four-membered ring transition state (i.e., similar to **TSB1** in Figure 9) in which it is difficult to maximize orbital overlaps between the proton, donor and acceptor atoms simultaneously. In relayed proton transfers, by contrast, both proton transfers can proceed with nearly linear arrangements of the protons, the donor and acceptor atoms (i.e., similar to **TSA1** in Figure 8), which lead to lower barriers. Although these previous calculations have emphasized the participation of extra water molecules in *dissociative* pathways of phosphate hydrolysis, we expect that the similar stereochemical argument to hold for associative mechanism as well; whether the process is fully concerted or stepwise[81] is not the essence of the problem. A major argument against the proton relay mechanism is that the organization of water molecules

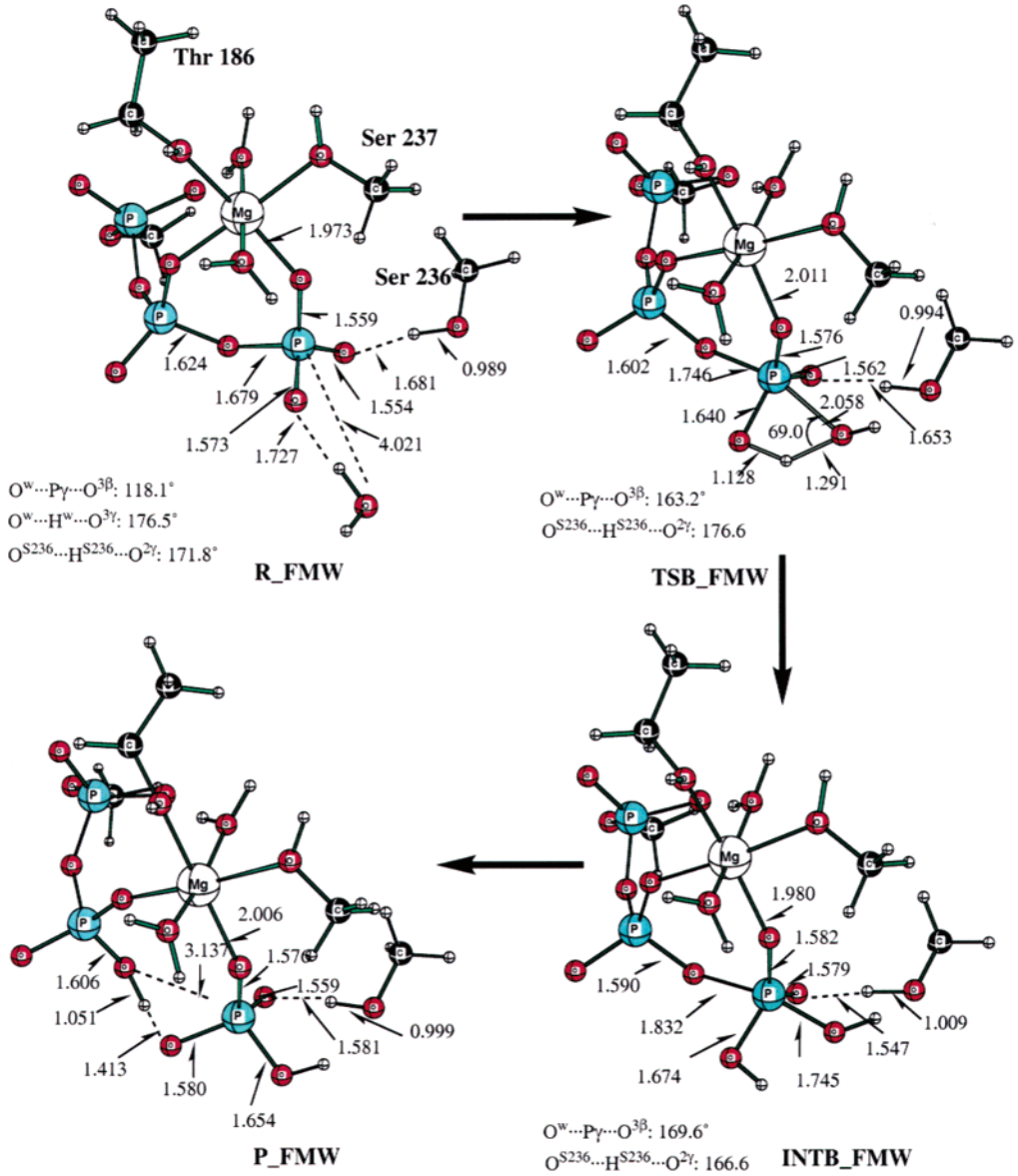

Figure 13. 13. Similar to Figure 8, but for path B1 when the motor domain is in the prehydrolysis state (1FMW).

into the specific orientation appropriate for proton relay is associated with a substantial amount of entropic penalty.[81] Although this is clearly true in solution (Cui et al., work in progress), we note that Ser236 is already well positioned to act as the relay group and therefore the relay mechanism is not expected to suffer from any significant entropic penalty in the myosin active site; more quantitative assessments require further calculations that include the fluctuations of the protein environment. We note that a recent QM/MM analysis of ATP hydrolysis in F_1−ATPase[82] found a similar trend as in the current study. That is, a two−water associative mechanism is energetically much more favorable than the single−water pathway, although different active site water molecules were used as the nucleophile in the comparison (we note that the energetics calculated in ref 82 are very endothermic, which is not consistent with the measured equilibrium constant of one[22] or the free energy perturbation calculations of Yang et al.[83] using a classical force field; the reason behind the discrepancy is not entirely clear, although one factor is that different X-ray structures were used in ref 82 and 83). In contrast to that study, however, the difference between path A and path B2 in myosin was found to be rather small (∼4 kcal/mol compared to ∼20 kcal/mol difference found in ref 82), especially considering the uncertainty associated with the present reaction path calculations. Therefore, we do not expect a spectacular change in the hydrolysis activity if Ser 236 is mutated to a residue that is incapable of relaying proton transfers. This is indeed the result of mutagenesis studies, which showed that Ser236A has rather normal hydrolysis activity.[33,35] Therefore, the fact that Ser 236 is conserved can be explained by the argument that it plays a significant role for the binding of ATP. Alternatively, it is possible that the Ser236A mutation introduces extra water molecules into the active site as the proton relay group; clearly, a high-resolution X-ray structure for the S236A mutant would be very useful to further clarify the role of Ser 236.

The calculated energetics for the slightly favored path A are only in fair agreements with experimental measurements, which is expected for a QM/MM reaction path analysis without including the thermal fluctuation of the protein environment. The hydrolysis products are nearly iso-energetic as the reactant state. This is consistent with the experimental observation that the equilibrium constant is nearly unity for the hydrolysis ($K < 10$),[19,22] which is sensible from energy transduction point of view (see below). The small equilibrium constant is also

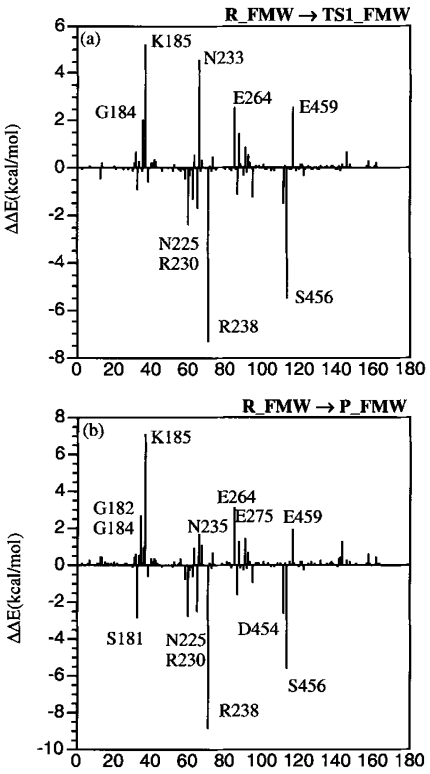

Figure 14. 14. Similar to Figure 11, but for path B1 when the motor domain is in the prehydrolysis state (1FMW).

consistent with the ^{18}O exchange experiments which showed rapid reversal of the hydrolysis.[84,85] The barriers calculated here are unfortunately substantially higher than experimental measurements; the calculated rate-limiting barrier for path A without zero-point corrections is 25.9 kcal/mol. Even if taking 2−3 kcal/mol zero-point correction into account, which is typical for proton-transfer reactions,[59] the barriers are still above 20 kcal/mol. Experimental measurements gave ATPase rate constants that range from 1 to 100 s^{-1},[22,38] which corresponds to free energy barriers in the range of 15−17 kcal/mol (converted based on transition state theory and a prefactor of kT/h at room temperature). The discrepancy between the calculations and experimental barrier cannot be clearly resolved here, and we will defer a more quantitative study using a more efficient QM/MM approach to the future. However, what is clear from the current study is that neither path A or path B2 has unreasonable energetics compared to experimental measurements. We note that our results are much closer to experimental measurements than any previous theoretical studies of myosin. For example, Okimoto et al.[78] calculated a barrier of 42 kcal/mol using a small active site model in the gas-phase based on a mechanism similar to path B. It was suggested that the high barrier is due to the neglect of the second active site water molecule,[50] but we suspect that the neglect of the protein environment in that study was the major limitation.

The roles of amino acids in the active site, in particular those in the switch I, switch II, and the P-loop region, have been analyzed with perturbation analysis. Although these analyses have been carried out for a limited configurations from reaction path calculations and thus are highly approximate, the results are qualitatively consistent with experiments including Lys 185,[33] Ser 181,[33] Asn 233,[35] Asn 235,[33,35] and Gly 457[32,34] (Figure 11). For Asp 454[32] and Ser 456,[34,38] more conformational sampling and actual mutant calculations have to be performed in the future to better understand their contributions.

In the elegant experiments of Hackney et al.,[86] it was found that although γ-oxygen atoms could undergo rapid exchange with the solvent, the bridging β-oxygen does not. This can be explained by the point that either the pentavalent intermediate does not break into ADP·Pi in the hydrolyzing state or the pseudorotation of the β-phosphate group is restricted due to coordination with Mg^{2+}. Both path A and path B studied here indicates that the pentavalent intermediate is high in energy and is separated from the reactant and product states with relatively small barriers. Therefore, we believe that the second explanation for the Hackney experiments is likely to be correct. Indeed, the bridging $O^{3\beta}$ is stabilized by several polar residues including Asn 233 and Gly 182, while $O^{2\beta}$ is coordinated to Mg^{2+}; it is sensible that such a tight coupling with the protein environment makes the pseudorotation of the β-phosphate group energy demanding. Potential of mean force calculations associated with the phosphate pseudorotation will be carried out to obtain more quantitative understandings. The rotational flexibility of the γ-phosphate in the ADP·Pi state also needs to be explored, because such flexibility is required to explain the rapid exchange of ^{18}O with the solvent.[84−86]

Another key goal of the current work is to understand the atomic details for the regulation of ATP hydrolysis, which is relevant to the mechanism of mechanochemical coupling in molecular motors in general.[7,8,87] In each functional cycle (e.g., myosin in Scheme 1), typically one ATP molecule in solution binds to the motor protein and is hydrolyzed, followed by the release of hydrolysis products back into solution. The net free energy change associated with the entire functional cycle is thus equivalent to the free energy of ATP hydrolysis in *solution* (Scheme 3), which is the free energy that the molecular motor can harness to generate useful work, although the actual hydrolysis obviously occurs in the *protein*. Since energy dissipation in proteins are on the pico-/nanosecond time scales without strongly preferred directions,[88,89] it is clear that it is not the free energies of the chemical reactions that are directly utilized. From this point of view, it is useful for the motor system to minimize the energy loss as heat. Therefore, an efficient system would have a very small energetical bias toward the hydrolysis products even when the system is in the *hydrolyzing* state (note especially in the functional cycle of myosin, as shown in Scheme 1, no work can be done *during* ATP hydrolysis because myosin is detached from actin), which is exactly what has been found experimentally for many motor systems (e.g., myosin, F_1−ATPase[19,90]). The computational results here are also consistent with these considerations. The key to the mechanochemical coupling, therefore, has to do with the connection of the protein structure and the ATP molecule in its various chemical states. Different conformations could be preferred with different ATP states (solvated ATP, bound ATP, hydrolysis transition state and ADP + Pi), and free energy is transferred between ATP and the protein/solvent through coupled conformational changes of the protein and binding/chemical modification of ATP. For motors with tracks, such as myosin and kinesin, interaction with the track also is an important element. For instance, as shown by the comparison between the actual processes and imaginary processes where the myosin−actin interaction is absent (Scheme 3), the binding energy provided by the actin is the key for an effective functional cycle; without the binding of actin, the system will get trapped kinetically in an intermediate state (e.g., M*·ADP·Pi).

Using the two high-resolution structures of myosin motor domains in different kinetic states, we were able to explore the coupling between the protein conformation and the ATPase

SCHEME 3. Schematic Free Energy for the Myosin-Actin System throughout One Function Cycle[a]

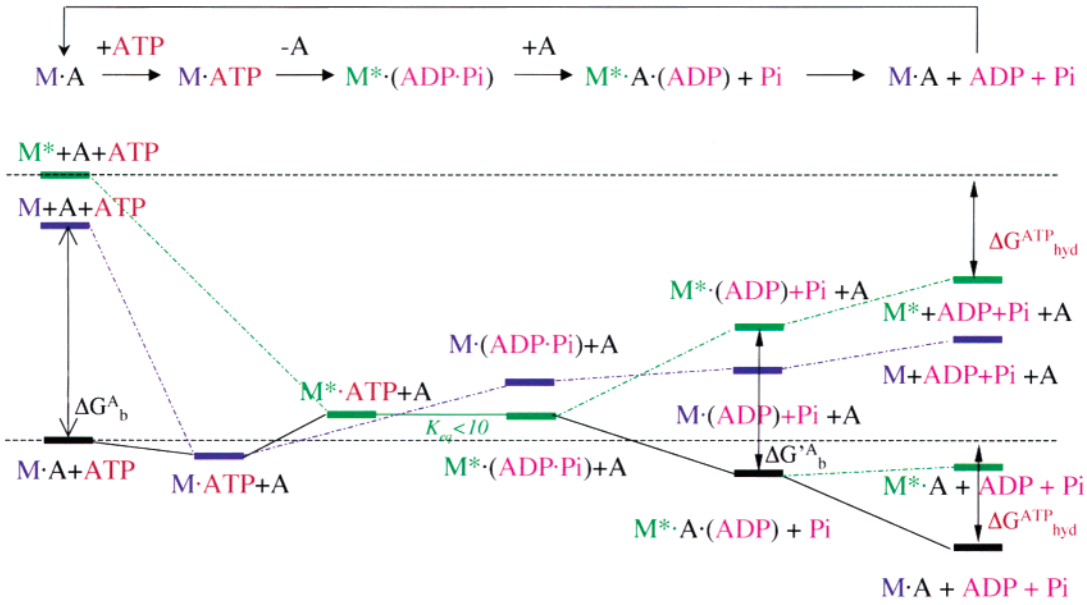

[a] The real processes are connected by solid lines, while imaginary processes are connected with dash-dotted lines; the latter are used to emphaize the importance of conformational change of the motor domain and the interaction with actin in achieving the mechanochemical coupling.

activity with atomic details. The calculations found high barriers and a large endothermicity for the ATP hydrolysis in 1FMW, which are consistent with the suggestion that 1FMW is in the prehydrolysis kinetic state and therefore is not capable of catalyzing ATP hydrolysis.[40] In the 1VOM structure, by contrast, the protein is in the conformation that favors ATP hydrolysis; the QM/MM calculations gave sensible barriers and an exothermicity of −0.4 kcal/mol for path A, which are consistent with those measured experimentally.[19,22] It was found that the regulation of ATP hydrolysis is largely due to the switch I and switch II regions in the active site. In the hydrolyzing state (1VOM), the two regions are stabilized by an important salt bridge between Arg 238 and Glu 459. This salt bridge is broken in the prehydrolysis state (1FMW), which has been shown by the present analysis to have both direct and indirect effects on the hydrolysis energetics. The direct effect is that, in 1FMW, Arg 238 and Ser 456 swing closer to the ATP, while Gly 457 and Glu 459 move away from the nucleotide (Figure 4). As a result, the ATP state is further stabilized and the product state is less stabilized with the prehydrolysis conformation (1FMW). However, perhaps more importantly, MD simulations clearly showed that the break of the salt bridge changes the water distribution and dynamics in the active site (Figure 5); as a result, the lytic water molecule is no longer maintained in configurations that favor in-line attacks as in the hydrolyzing conformation (1VOM). These combined effects make the nucleophilic attack barrier very high in the prehydrolysis state. The critical role of the salt bridge is consistent with mutation studies,[33−35,49,50] which showed that mutating either Arg 238 or Glu 459 decreased the hydrolysis activity substantially, while the double mutant R238E/E459R is well capable of catalyzing ATP hydrolysis.

IV. Conclusions

Classical molecular dynamics and combined QM/MM reaction path calculations have been used to explore the catalytic and regulatory mechanisms of ATP hydrolysis in myosin-II. These two complementary techniques have yielded useful insights into different aspects of the hydrolysis cycle, and the results have general implications for the mechanochemical coupling in motor proteins in general.

Among the two associative mechanisms studied here, the QM/MM reaction path calculations with the appropriate hydrolyzing conformation of the myosin motor domain (PDB code 1VOM) showed that path A has a lower rate-limiting barrier than path B; the former involves Ser 236 as the relaying group for the proton transfer from the lytic water to the γ-phosphate, while the latter involves a direct proton transfer without relays. Therefore, it is likely that path A is the preferred mechanism in wild-type myosin, which is consistent with the fact that Ser 236 is a conserved residue. Perturbation analyses suggested that the major difference between path A and path B is not due to any specific protein residues but to the intrinsic difference in the stereochemistry associated with the two pathways. However, we also note that if $O^{2\gamma}$ is protonated in path B (path B2), the rate-limiting barrier is not much higher than path A. Considering the limited accuracy of the present QM/MM reaction path calculations, which have not taken the thermal fluctuations of the protein into account, it is difficult to exclude the possibility that path B2 also contributes to the hydrolysis mechanism. As a matter of fact, this interpretation is qualitatively consistent with the experimental result that Ser 236A mutant has only slightly reduced (∼25%) ATP hydrolysis rate.[33,35] Despite the remaining uncertainty in the hydrolysis mechanism, our contribution is having shown that sensible energetics for the hydrolysis reaction (activation barrier, exothermicity of the hydrolysis and contribution from active site residues) can be obtained once the influence from the protein environment is appropriately taken into account; the much higher barrier found in previous work is most likely due to the neglect of the protein environment in the calculations.[78]

A particularly encouraging result is that QM/MM calculations correctly reproduced the trend that ATP hydrolysis has much higher barrier and endothermicity with the prehydrolysis conformation of the motor domain (PDB structure 1FMW), which is consistent with the notion that the prehydrolysis conformation is not capable of catalyzing ATP hydrolysis. The current analysis indicated that the conformational regulation of

ATP hydrolysis in myosin is largely determined by several residues in the switch I and switch II regions. In particular, the salt bridge between Arg 238 and Glu 459, which is broken in 1FMW, was shown to have both direct and indirect effects. The Arg 238 is closer to ATP in 1FMW than in 1VOM, which makes the ATP state more stabilized than the hydrolysis products (ADP•Pi). Furthermore, classical MD simulations clearly showed that water structures in the active site are different in the two motor conformations. In 1VOM, the salt bridge between Arg 238 and Glu 459 helps to stabilize the water structure in which the lytic water has nearly perfect in-line attack conformation. In 1FMW, by contrast, the salt bridge is broken, and therefore, water molecules undergo large fluctuations and on average do not have the appropriate position for in-line attacks, which also makes the hydrolysis reaction highly unfavorable.

The current work represents our *initial* efforts to understand the atomic details of mechanochemical coupling in molecular motors. Further studies are required to generate a more complete understanding and to confirm the current analysis. For example, there are still other possible mechanisms for the hydrolysis, such as the dissociative pathway. Although previous theoretical studies by Warshel and co-workers found that dissociative and associative pathways are close in energies in Ras p21,[91−93] the structure of the ADP•vanadate structure suggests that the associative pathway is very likely; this certainly cannot exclude the dissociative pathway. Although γ-phosphate being the general base for its hydrolysis seems widely accepted in the myosin field since there is no general base within 5 Å, the issue remains controversial in the general area of phosphate hydrolysis and one might indeed envision other pathways for generating a nucleophilic OH^- group. For example, it has been suggested that Glu 459 may act as the general base through the hydrogen-bond network involving water molecules.[50] Finally, a recent Car−Parrinello simulation found that Lys 185 protonates the γ-phosphate in a spontaneous fashion within 150 fs of MD, which led the authors to the suggestion that Lys 185 can act as the general acid that catalyzes the hydrolysis;[48] it has been commented that,[14] however, the observed proton transfer might be an artifact due to the small number of protein residues explicitly included in that simulation. The present study has not addressed these possibilities, because these mechanisms involve more significant perturbations to the active site structure, and therefore a reaction path QM/MM study is not sufficient. Also not explored are other possible protonation patterns associated with ATP, ADP/Pi, and the ligands of the Mg^{2+} ion; e.g., given the pK_a's sufficiently close to 7, ATP might be protonated, and one of the ligands (Thr 185, Ser 237) might be deprotonated. Model studies of monophosphate hydrolysis found that the energetics of associative pathway are rather similar for mono-anionic and doubly anionic phosphates.[47] All these issues need to be explored in more details in the future using SCC-DFTB/CHARMM,[75] which is sufficiently fast and allows adequate conformational samplings.[94] In terms of the conformational regulation of ATP hydrolysis, a free energy perturbation study has been carried out to complement the QM/MM reaction path analysis; the overall trends were very consistent in the two studies. Finally, much more studies are required to understand the mechanisms of conformational transitions in the motor domains and, perhaps more importantly, the effect of myosin−actin interaction on the binding properties of ATP, ADP, and Pi.

As a final note, it is interesting to consider the mechanochemical coupling in molecular motors as a special case of "dynamical disorder" in catalysis.[95] Elegant single molecule studies have revealed that many enzymes have slow fluctuations in their conformations that modulate the kinetics of the chemical reaction being catalyzed.[96−98] Structural details for such slow fluctuations, in most cases, however, remain to be elucidated. Molecular motors are great systems to explore dynamical disorders because structural fluctuations have a major impact on the chemistry and is a key characteristic of the system (in contrast to, for example, cholesterol oxidase,[96] where the variation in rate was found to be less than a factor of 10), which might make it easier to analyze the identity of the slow fluctuations.

Acknowledgment. The Q.C. group is partially supported by the starting-up fund from the Department of Chemistry and College of Letters and Science at University of Wisconsin, Madison, a PRF-G grant from the donors of the Petroleum Research Fund, administered by the American Chemical Society, and a Research Innovation Award from the Research Corp. We thank Prof. I. Rayment, S. Gilbert and D. Hackney for discussions and encouragements.

References and Notes

(1) Alberts, B.; Bray, D.; Lewis, J.; Raff, M.; Roberts, K.; Watson, J. D. *Molecular biology of the Cell*, 3rd. ed.; Garland Publishing: New York and London, 1994.

(2) Keike, M. C.; Titus, M. A. In *Molecular Motors*; Schliwa, M., Ed.; Wiley-VCH: Munchen, Germany, 2003.

(3) Hirokawa, N.; Takemura, R. In *Molecular motors*; Schliwa, M., Ed.; Wiley-VCH: Munchen, Germany, 2003.

(4) Lee, A. G.; East, J. M. *Biochem. J.* **2001**, *356*, 665−683.

(5) Gao, Y.; Yang, W.; Marcus, R. A.; Karplus, M. *Proc. Natl. Acad. Sci. U.S.A.* **2003**, *100*, 11339−11344.

(6) Strajbl, M.; Shurki, A.; Warshel, A. *Proc. Natl. Acad. Sci. U.S.A.* **2003**, *100*, 14834−14839.

(7) Vale, R. D.; Milligan, R. A. *Science* **2000**, *288*, 88−95.

(8) Bustamante, C.; Keller, D.; Oster, G. *Acc. Chem. Res.* **2001**, *34*, 412−420.

(9) Karplus, M.; McCammon, J. A. *Nature, Struct. Biol.* **2002**, *9*, 646−652.

(10) Field, M. J.; Bash, P. A.; Karplus, M. *J. Comput. Chem.* **1990**, *11*, 700−733.

(11) Gao, J. In *Reviews in Computational Chemistry*; Lipkowitza, K. B., Boyd, D. B., Eds.; VCH: New York, 1996; Vol. 7, p 119.

(12) Gao, J.; Truhlar, D. G. *Annu. Rev. Phys. Chem.* **2002**, *53*, 467−505.

(13) Åqvist, J.; Warshel, A. *Chem. Rev.* **1993**, *93*, 2523.

(14) Warshel, A. *Annu. Rev. Biophys. Biomol.* **2003**, *32*, 425−443.

(15) Li, G.; Cui, Q. *Biophys. J.* **2004**, *86*, 743.

(16) Li, G.; Cui, Q. *Biophys. J.* **2002**, *83*, 2457−2474.

(17) Cui, Q.; Li, G.; Ma, J.; Karplus, M. *J. Mol. Biol.* **2003**, submitted for publication.

(18) Bagshaw, C. R. In *Molecular Motors*; Banting, G., Higgins, S. J., Eds.; Portland Press: London, 2000; Vol. 35, pp 19−31.

(19) Holmes, K. C.; Geeves, M. A. *Annu. Rev. Biochem.* **1999**, *68*, 687−728.

(20) Sablin, E. P.; Fletterick, R. J. *Curr. Opin. Struct. Biol.* **2001**, *11*, 716−724.

(21) Lymn, R. W.; Taylor, E. W. *Biochemistry* **1971**, *10*, 4617−4624.

(22) Trentham, D. R.; Eccleston, J. F.; Bagshaw, C. R. *Q. Rev. Biophys.* **1976**, *9*, 217−281.

(23) Rayment, I. *J. Biol. Chem.* **1996**, *271*, 15850−15853.

(24) Rayment, I.; Holden, H. W.; Whitaker, M.; Yohn, C. B.; Lorenz, M.; Holmes, K. C.; Milligan, R. A. *Science* **1993**, *261*, 58−61.

(25) Houdusse, A.; Sweeney, H. L. *Curr. Opin. Struct. Biol.* **2001**, *11*, 182−194.

(26) Houdusse, A.; Szent-Gyorgyi, A. G.; Cohen, C. *Proc. Natl. Acad. Sci. U.S.A.* **2000**, *97*.

(27) Reubold, T. F.; Eschenburg, S.; Becker, A.; Kull, F. J.; Manstein, D. J. *Nature, Stuct. Biol.* **2003**, *10*, 826−830.

(28) Gourinath, S.; Himmel, D. M.; Brown, J. H.; Reshetnikova, L.; Szent-Gyorgyi, A. G.; Cohen, C. *Structure* **2003**, *11*, 1621−1627.

(29) Coureux, P.; Wells, A. L.; Menetrey, J.; Yengo, C. M.; Morris, C. A.; Sweeney, H. L.; Houdusse, A. *Nature (London)* **2003**, *425*, 419−423.

(30) Whittaker, M.; Wilsonkubalek, E. M.; Smith, J. E.; Faust, L.; Milligan, R. A.; Sweeney, H. L. *Nature (London)* **1995**, *378*, 748−751.

(31) Holmes, K. C.; Angert, I.; Kull, F. J.; Jahn, W.; Schroder, R. R. *Nature* **2003**, *425*, 423−427.
(32) Kambara, T.; Rhodes, T. E.; Ikebe, R.; Tamada, M.; White, H. D.; Ikebe, M. *J. Biol. Chem.* **1999**, *274*, 16400−16406.
(33) Li, X.; Rhodes, T. E.; Ikebe, R.; Kambara, T.; White, H. D.; Ikebe, M. *J. Biol. Chem.* **1998**, *273*, 27404−27411.
(34) Sasaki, N.; Shimada, T.; Sutoh, K. *J. Biol. Chem.* **1998**, *273*, 20334−20340.
(35) Shimada, T.; Sasaki, N.; Ohkura, R.; Sutoh, K. *Biochemistry* **1997**, *36*, 14037−14043.
(36) Ishijima, A.; Kojima, H.; Funatsu, T.; Tokunaga, M.; Higuchi, H.; Tanaka, H.; Yanagida, T. *Cell* **1998**, *92*, 161−171.
(37) Ishii, Y.; Kitamura, K.; Tanaka, H.; Yanagida, T. *Methods Enzymol.* **2003**, *361*, 228−245.
(38) Murphy, C. T.; Rock, R. S.; Spudich, J. A. *Nature, Cell Biol.* **2001**, *3*, 311−315.
(39) Steffen, W.; Smith, D.; Sleep, J. *Proc. Natl. Acad. Sci. U.S.A.* **2003**, *100*, 6434−6439.
(40) Bauer, C. B.; Holden, H. W.; Thoden, J. B.; Smith, R.; Rayment, I. *J. Biol. Chem.* **2000**, *275*, 38494−38499.
(41) Bohm, A.; Gaudet, R.; Sigler, P. B. *Curr. Opin. Biotechnol.* **1997**, *8*, 480−487.
(42) Gulick, A. M.; Bauer, C. B.; Thoden, J. B.; Rayment, I. *Biochemistry* **1997**, *36*, 11619−11628.
(43) Fisher, A. J.; Smith, C. A.; Thoden, J. B.; Smith, R.; Sutoh, K.; Holden, H. W.; Rayment, I. *Biochemistry* **1995**, *34*, 8960−8972.
(44) Smith, C. A.; Rayment, I. *Biochemistry* **1996**, *35*, 5404−5417.
(45) Dominguez, R.; Freyzon, Y.; Trybus, K. M.; Cohen, C. *Cell* **1998**, *94*, 559−571.
(46) Hu, C. H.; Brinck, T. *J. Phys. Chem. A* **1999**, *103*, 5379−5386.
(47) Wang, Y.; Topol, I. A.; Collins, J. R.; Burt, S. K. *J. Am. Chem. Soc.* **2003**, *125*, 13265−13273.
(48) Minehardt, T. J.; Marzari, N.; Cooke, R.; Pate, E.; Kollman, P. A.; Car, R. *Biophys. J.* **2002**, *82*, 660−675.
(49) Onishi, H.; Kojima, H.; Katoh, K.; Fujiwara, K.; Martinez, H. M.; Morales, M. F. *Proc. Natl. Acad. Sci. U.S.A.* **1998**, *95*, 6653−6658.
(50) Onishi, H.; Ohki, T.; Mochizuki, N.; Morales, M. F. *Proc. Natl. Acad. Sci. U.S.A.* **2002**, *99*, 15339−15344.
(51) Brooks, C. L., III; Brünger, A.; Karplus, M. *Biopolymer* **1985**, *24*, 843.
(52) Brooks, C. L., III; Karplus, M. *J. Chem. Phys.* **1983**, *79*, 6312−6325.
(53) Brooks, C. L., III; Karplus, M. *J. Mol. Biol.* **1989**, *208*, 159−181.
(54) Ryckaert, J. P.; Ciccotti, G.; Berendsen, H. J. *J. Comput. Phys.* **1977**, *23*, 327−341.
(55) Brooks, B. R.; Bruccoleri, R. E.; Olafson, B. D.; States, D. J.; Swaminathan, S.; Karplus, M. *J. Comput. Chem.* **1983**, *4*, 187−217.
(56) MacKerell, A. D., Jr.; Bashford, D.; Bellott, M.; Dunbrack, R. L., Jr.; Evanseck, J. D.; Field, M. J.; Fischer, S.; Gao, J.; Guo, H.; Ha, S.; Joseph-McCarthy, D.; Kuchnir, L.; Kuczera, K.; Lau, F. T. K.; Mattos, C.; Michnick, S.; Ngo, T.; Nguyen, D. T.; Prodhom, B.; Reiher, W. E., III; Roux, B.; Schlenkrich, M.; Smith, J. C.; Stote, R.; Straub, J.; Watanabe, M.; Wiorkiewicz-Kuczera, J.; Yin, D.; Kraplus, M. *J. Phys. Chem. B* **1998**, *102*, 3586−3616.
(57) Bashford, D.; Karplus, M. *Biochem.* **1990**, *29*, 10219−10225.
(58) Simonson, T.; Archontis, G.; Karplus, M. *J. Phys. Chem. B* **1997**, *101*, 8349−8362.
(59) Cui, Q.; Karplus, M. *J. Am. Chem. Soc.* **2001**, *122*, 2284−2290.
(60) Reuter, N.; Dejaegere, A.; Maigret, B.; Karplus, M. *J. Phys. Chem. A* **2000**, *104*, 1720−1735.
(61) Szabo, A.; Ostlund, N. S. *Modern quantum chemistry−introduction to advanced electronic structure theory*; Dover Publications: New York, 1989.
(62) Binkley, J. S.; Pople, J. A.; Hehre, W. J. *J. Am. Chem. Soc.* **1980**, *102*, 939.
(63) Gordon, M. S.; Binkley, J. S.; Pople, J. A.; Peitro, W. J.; Hehre, W. J. *J. Am. Chem. Soc.* **1982**, *104*, 2797.
(64) Becke, A. D. *J. Chem. Phys.* **1993**, *98*, 5648−5652.
(65) Becke, A. D. *Phys. Rev. A* **1998**, *38*, 3098−3100.
(66) Lee, C.; Yang, W.; Parr, R. G. *Phys. Rev. B* **1988**, *37*, 785−789.
(67) Hariharan, P. C.; Pople, J. A. *Theor. Chim. Acta* **1973**, *28*, 213−222.
(68) Krishnan, R.; Binkley, J. S.; Seeger, R.; Pople, J. A. *J. Chem. Phys.* **1980**, *72*, 650−654.
(69) Brooks, C. L., III; Karplus, M.; Pettitt, B. M. *Proteins: A Theoretical Perspective of Dynamics, Structure, & Thermodynamics*; John Wiley & Sons: 1988; Vol. LXXI.
(70) Fischer, S.; Karplus, M. *Chem. Phys. Lett.* **1992**, *194*, 252−261.
(71) Cui, Q.; Karplus, M. *J. Am. Chem. Soc.* **2002**, *124*, 3093−3124.
(72) Cui, Q.; Karplus, M. *J. Phys. Chem. B* **2002**, *106*, 1768.
(73) Strajbl, M.; Hong, G.; Warshel, A. *J. Phys. Chem. B* **2002**, *106*, 13333−13343.
(74) Olsson, M. H. M.; Hong, G.; Warshel, A. *J. Am. Chem. Soc.* **2003**, *125*, 5025−5039.
(75) Cui, Q.; Elstner, M.; Kaxiras, E.; Frauenheim, T.; Karplus, M. *J. Phys. Chem. B* **2001**, *105*, 569−585.
(76) Li, G.; Cui, Q. *J. Phys. Chem. B* **2003**, *107*, 8643−8653.
(77) Li, G.; Cui, Q. *J. Am. Chem. Soc.* **2003**, *125*, 15028−15038.
(78) Okimoto, N.; Yamanaka, K.; Ueno, J.; Hata, M.; Hoshino, T.; Tsuda, M. *Biophys. J.* **2001**, *81*, 2786−2794.
(79) Lahiri, S. D.; Zhang, G.; Dunaway-Mariano, D.; Allen, K. N. *Science* **2003**, *299*.
(80) Bash, P. A.; Field, M. J.; Davenport, R. C.; Petsko, G. A.; Ringe, D.; Karplus, M. *Biochemistry* **1991**, *30*, 5826−5832.
(81) Schweins, T.; Warshel, A. *Biochemistry* **1996**, *35*, 14232−14243.
(82) Dittrich, M.; Hayashi, S.; Schulten, K. *Biophys. J.* **2003**, *85*, 2253−2266.
(83) Yang, W.; Gao, Y.; Cui, Q.; Ma, J.; Karplus, M. *Proc. Natl. Acad. Sci. U.S.A.* **2003**, *100*, 874−879.
(84) Bagshaw, C. R.; Trentham, D. R.; Wolcott, R. G.; Boyer, P. D. *Proc. Natl. Acad. Sci. U.S.A.* **1975**, *72*, 2592−2596.
(85) Webb, M. R.; Trentham, D. R. *J. Biol. Chem.* **1981**, *256*, 10910−10916.
(86) Dale, M. P.; Hackney, D. D. *Biochem.* **1987**, *26*, 8365−8372.
(87) Rees, D. C.; Howard, J. B. *J. Mol. Biol.* **1999**, *293*, 343−350.
(88) Wang, Q.; Wong, C. F.; Rabitz, H. *Biophys. J.* **1998**, *75*, 60−69.
(89) Sagnella, D. E.; Straub, J. E. *J. Phys. Chem. B* **2001**, *105*, 7057−7063.
(90) Boyer, P. D. *Biochim. Biophys. Acta* **1993**, *1140*, 215−250.
(91) Florian, J.; Warshel, A. *J. Phys. Chem. B* **1998**, *102*, 719−734.
(92) Glennon, T. M.; Villa, J.; Warshel, A. *Biochemistry* **2000**, *39*, 9641−9651.
(93) Aqvist, J.; Kolmodin, K.; Florian, J.; Warshel, A. *Chem. Biol.* **1999**, *6*, R71−R80.
(94) Cui, Q.; Elstner, M.; Karplus, M. *J. Phys. Chem. B* **2002**, *106*, 2721−2740.
(95) Karplus, M. *J. Phys. Chem.* **2000**, *104*, 11−27.
(96) Lu, H. P.; Xun, L.; Xie, X. *Science* **1998**, *282*, 1877.
(97) Xie, X.; Lu, H. P. *J. Biol. Chem.* **1999**, *274*, 15967.
(98) Xie, X. *J. Chem. Phys.* **2002**, *117*, 11024−11032.